The Fe (III) / Fe(II) Redox Couple as a Probe of Immobilized Tobacco Peroxidase: Effect of the Immobilization Protocol

José Luis Olloqui-Sariego,[a] Galina S. Zakharova,[b] Andrey A. Poloznikov,[b] Juan José Calvente,[a] Dmitry M. Hushpulian,[b] Lo Gorton,[c] Rafael Andreu [a,*]

[a] Department of Physical Chemistry. University of Sevilla. Profesor García González 1. 41012 Sevilla. Spain.

[b] D. Rogachev center of Pediatric Hematology, Oncology and Immunology, 1 Samory Mashela str., Moscow 117997, Russia.

[c] Department of Biochemistry and Structural Biology. Lund University, P. O. Box 124, 221 00, Lund, Sweden.

[*]Corresponding author's e-mail: fondacab@us.es

Abstract

Non-turnover voltammetry is a sensitive tool to characterize the electrochemical properties of redox proteins. However, the catalytically competent oxidation states of most peroxidases do not display the required electrochemical reversibility. In this report, we circumvent this limitation and exploit the voltammetric response associated with the *Fe(III)/Fe(II)* redox couple of tobacco peroxidase to probe the energetics and electronic connectivity of the heme pocket. We have applied this approach to rationalize the previously reported influence of the immobilization protocol on the electrocatalytic activity of tobacco peroxidase. To decouple proton and electron transfer steps, measurements have been carried out over the $3 \leq pH \leq 9$ range and a $1e^-/2H^+$ ladder scheme has been adopted for their analysis. At each pH, thermodynamic and kinetic parameters associated with the *Fe(III)*/*Fe(II)* redox conversion were determined as a function of temperature in the 0-30ºC range. Reduction entropies and reorganization energies displayed different values for covalently immobilized and physisorbed enzymes, pointing to a larger involvement of the solvent in the last case. These findings, together with a larger electronic coupling between the prosthetic group and the electrode, are indicative of a partial denaturation of the physisorbed enzymes as the origin of their lower electrocatalytic activity.

Keywords: Tobacco Peroxidase; Proton Coupled Electron Transfer; Fe(III)/Fe(II) Couple; Immobilization Protocol; Thermodynamics and Kinetics

1. Introduction

Peroxidases are heme enzymes that catalyze the oxidation of a wide variety of organic and inorganic substrates by peroxides. Their catalytic function involves the oxidation of the heme iron to *Compound I*, which is then reduced by the substrate to *Compound II* and *Fe(III)* in two consecutive electron transfer steps [1]. Anionic tobacco peroxidase (*TOP*) is a class III plant peroxidase, which has been recognized as a promising building block for biosensors due to its high stability and substrate specificity [2,3]. When peroxidases are integrated in mediatorless electrocatalytic devices, such as third generation biosensors, an electrode replaces the substrate as the source of electrons to reduce *Compound I* and *Compound II* [4,5]. To generate a reliable response, this configuration requires that electroactive enzymes preserve their tertiary structure around the catalytic pocket after immobilization, and that redox cofactors are adequately wired to the electrode surface [6].

A number of studies have described both direct and mediated electrocatalytic responses of tobacco peroxidase adsorbed on a variety of electrode surfaces [7−16], but little is known on the impact of the enzyme immobilization protocol on the redox properties of the heme cofactor. Recently, we have shown that the covalent immobilization of crosslinked *TOP* oligomers (*ci-olig-TOP*) on a graphite electrode results in a significant improvement of the recorded electrocatalytic currents, as compared to those produced by covalently immobilized (*ci-mon-TOP*) and physically adsorbed (*pa-mon-TOP*) *TOP* monomers [14]. To explore the origin of this behavior, non-turnover voltammetry provides a simple and effective method to probe the electronic wiring and energetics of the redox center of immobilized enzymes [17]. However, this type of analysis can only be applied to the *Fe(III)*/*Fe(II)* redox couple of the heme center since the higher oxidation states involved in the catalytic cycle of

peroxidases do not provide a reversible voltammetric response under non-turnover conditions, except in the case of cytochrome *c* peroxidase [18,19].

Our previous voltammetric study of immobilized *TOP* was performed at pH 7 and 0ºC, where the three aforementioned immobilization protocols produced similar non-turnover voltammograms, in stark contrast with their distinct electrocatalytic responses [14]. In this work we have carried out a systematic analysis of the influence of pH and temperature on the *Fe(III)/Fe(II)* redox conversion of immobilized *TOP* enzymes. Though only c.a. one fifth of the electroactive heme groups of covalently immobilized *TOP* enzymes retain their ability to reduce hydrogen peroxide via the *Compound I*/*Compound II*/*Fe(III)* catalytic cycle [15], a single and characteristic *Fe(III)/Fe(II)* voltammetric response is observed for each immobilization protocol. To decouple the contributions from proton and electron transfer steps we have adopted a $1e^-/2H^+$ ladder scheme, where proton steps are assumed to remain in equilibrium. Proton coupling is shown to lead to a pH dependent contribution to the reduction entropy of the enzyme, which may help to explain the broad range of reduction entropy values reported in literature for peroxidases [20]. The effect of temperature on the thermodynamic and kinetic charge transfer parameters is observed to be different for physisorbed and chemisorbed enzymes, and delineates a physical scenario where physisorbed enzymes undergo conformational changes that may explain their loss of electrocatalytic activity.

2. Material and methods

2.1. Enzyme production

Wild-type recombinant *TOP* (hydrogen peroxide oxidoreductase, EC 1.11.1.7) was expressed in the form of inclusion bodies in *E. coli* BL21(DE3) CodonPlus cells as was

described earlier [21]. The construction of the expression vector and the procedure of *TOP* expression, refolding and purification are covered in detail elsewhere [21]. Briefly, the biomass from 600 mL of culture medium was disrupted, and the precipitate of inclusion bodies was washed, solubilized in 6 M urea and added drop by drop to the refolding medium, containing 1.8 M urea, 0.1 mM DTT, 0.5 mM oxidized glutathione, 3 mM $CaCl_2$, 5 µM hemin and 5% glycerol in 50 mM Tris-HCl pH 9.5. After *in vitro* reactivation, *r*-TOP was concentrated and purified on a Toyopearl HW-55 column. The concentration of peroxidase was measured by the absorbance at 403 nm, using the experimentally determined extinction coefficient value of 108.0 ± 0.5 $mM^{-1}cm^{-1}$ for the protein monomer [22]. The resulting preparation was homogeneous as judged by SDS-PAGE. The activity of purified *TOP* towards ABTS was about 4100 U/mg and the RZ value was 3.0.

2.2. Reagents

1-Ethyl-3-(3-dimethylaminopropyl) carbodiimide (EDC) and N-hydroxy sulfosuccinimide sodium salt (NHS) were from Sigma-Aldrich. Sodium phosphate buffer solutions (SPB) of fixed ionic strength were prepared from phosphoric acid, and mono and dihydrogen sodium phosphate from Fluka, and sodium perchlorate and sodium hydroxide from Sigma-Aldrich. All reagents were of high purity, and were used as received. Water was purified with a Millipore Milli-Q system (resistivity 18 MΩ cm).

2.3. Enzyme immobilization

Pyrolytic graphite electrodes were constructed by fitting a rod of highly oriented pyrolytic graphite from Mineral Technologies into a PEEK casing, so that it exposed the edge of the graphite planes with a circular geometric area of 0.07 cm^2. Prior to enzyme

immobilization, graphite surfaces were polished with abrasive P2400 sandpaper, rinsed with Millipore water and dried with an argon stream.

To physisorb *TOP*, a 17 µL drop of 0.11 mg mL^{-1} *TOP* in 0.01 M SPB pH 6 was deposited on the graphite surface, and physisorption from solution was allowed to proceed for 20 h at 4ºC under wet conditions.

For covalent coupling of *TOP* monomers, the electrode was incubated for 2 h at 4ºC in a solution formed by mixing a 4.5 µL drop of 20 mM NHS and a 5.5 µL drop of 40 mM EDC, both solutions being also 0.01 M SPB pH 6. After activation of the oxidized species at the graphite surface, the electrode was thoroughly rinsed with water and dried with an argon stream. Then, in a second incubation step that lasted 20 h at 4ºC, the electrode was capped with a 17 µL drop of a 0.11 mg mL^{-1} *TOP* solution in 0.01 M SPB pH 6.

For covalent trapping of *TOP* oligomers the electrode surface was exposed to a mixture of three droplets: a 4.5 µL drop of 20 mM NHS, a 5.5 µL drop of 40 mM EDC and 7 µL drop of a 0.26 mg mL^{-1} *TOP* solution, that were also 0.01 M SPB pH 6, for 20 h at 4ºC.

Irrespective of the immobilization protocol, the enzyme concentration in the deposition solution was 3 µM, and the electrodes were thoroughly rinsed, first with water and then with the working buffer solution, after enzyme incubation.

2.4. Electrochemical measurements

All electrochemical measurements were performed with an AUTOLAB PGSTAT 30, from Eco Chemie B.V, in a conventional three electrode undivided glass cell, equipped with a gas inlet and thermostated with a water jacket. The counter and reference

electrodes were a Pt bar and a Ag|AgCl|NaCl saturated electrode, respectively. The reference electrode was connected to the cell solution via a salt bridge, and kept at room temperature (23 ± 2ºC) in a non-isothermal configuration. Reported potential values have been referred to the SHE potential scale by adding +192 mV to the experimental potential values. All measurements were carried out under argon atmosphere. Working solutions contained 0.02 M sodium phosphate buffer at the desired pH plus sodium perchlorate to adjust the ionic strength to 0.12 M. Positive feedback for ohmic drop compensation was applied whenever the potential scan rate was higher than 1 V s^{-1}.

3. Results and discussion

3. 1. Impact of Solution pH on the Fe(III) / Fe(II) redox conversion of TOP

Figure 1 illustrates some voltammetric characteristics of immobilized TOP under non-turnover conditions at 25ºC. A couple of surface voltammetric waves, associated with the *Fe(III)/Fe(II)* redox conversion, can be observed at potentials close to 0 V at pH 3. As the solution is made more basic, the waves shift towards more negative potentials (see Figure 1a), indicating that the redox process is accompanied by proton exchange with solution. The surface concentration of electroactive heme groups, as determined by integration of the baseline corrected voltammograms, was found to lie within 80 ± 20 pmol cm^{-2} for *ci-olig-TOP* and *pa-mon-TOP*, and within 40 ± 10 pmol cm^{-2} for *ci-mon-TOP*. The full width at half maximum of the peaks at low scan rate (typically between 150 mV and 200 mV) is larger than the value expected for a population of identical non-interacting redox centers (90.6 mV at 25ºC), suggesting the presence of a variety of environments around the heme groups, including the possibility of conformational changes that may affect the catalytic activity of the enzymes. The

peak potential separation ΔE_p remains insensitive to the potential scan rate *v* up to 10 V s^{-1}, which is indicative of a fast electron exchange between protein and electrode [23].

Irrespective of the immobilization protocol, the midpoint potential $E_{1/2}$ (determined from the average of the anodic and cathodic peak potentials) varies linearly with pH in basic solutions, it reaches a plateau for pH values close to 5, and it increases again as the solution is made more acidic (see Figure 1b). Previously reported $E_{1/2}$ values for physisorbed *TOP* at pH 5 [13] and 7 [14] are in good agreement with those displayed in Figure 1b. The shape of these $E_{1/2}$ vs pH curves is analogous to that of the potentiometric titration curves of isoenzymes C and A of horseradish peroxidase (*HRP*), though they are shifted towards more acidic pHs and more positive potentials in relation to those of *HRP-C* [24] and *HRP-A* [25]. The simplest reaction scheme that can describe the observed variation of the midpoint potential with pH is a six membered ladder-scheme (see Scheme 1), involving two acid/base groups A_1 and A_2 whose acid dissociation equilibrium constants are dependent on the oxidation state of the heme group, and are denoted as $K_{ox,1}$, $K_{ox,2}$, $K_{red,1}$ and $K_{red,2}$ [26,27]. Moreover, the three protonation states of the oxidized heme are related to their corresponding reduced forms through three electron transfer steps, each one being characterized by its formal potential E_i^f and standard rate constant of electron transfer $k_{s,i}$ (*i* = 1, 2, 3). According to this reaction scheme, three plateaus corresponding to $E_{1/2} = E_1^f$, $E_{1/2} = E_2^f$ and $E_{1/2} = E_3^f$ are to be expected in a $E_{1/2}$ vs pH plot when the electron transfer takes place sequentially through each of the three parallel electron pathways, as the solution is made more basic, according to:

$$E_{1/2} = E_2^f + \frac{RT}{F} \ln \frac{\left(c_{H^+} / K_{red,1}\right) + 1 + \left(K_{red,2} / c_{H^+}\right)}{\left(c_{H^+} / K_{ox,1}\right) + 1 + \left(K_{ox,2} / c_{H^+}\right)} \qquad (1)$$

where c_{H^+} is the proton concentration in solution, *R*, *T* and *F* have their usual meaning, and the other symbols are defined in Scheme 1. The two extreme plateaus associated with electron exchange between fully protonated ($E_{1/2} = E_1^f$) or deprotonated ($E_{1/2} = E_3^f$) species are not observed in the pH range we have explored, and only the intermediate plateau is clearly noticed (Figure 1b). Therefore, the redox process takes place through the shaded pathway in Scheme 1 under the present working conditions, and neither the doubly protonated oxidized form nor the doubly deprotonated reduced form dominate their respective oxidation states. Then, $\left(c_{H^+} / K_{ox,1}\right) << 1$, $\left(K_{red,2} / c_{H^+}\right) << 1$ and eq. (1) simplifies to:

$$E_{1/2} = E_2^f + \frac{RT}{F} \ln \frac{\left(c_{H^+} / K_{red,1}\right) + 1}{1 + \left(K_{ox,2} / c_{H^+}\right)} \qquad (2)$$

This expression reproduces satisfactorily the observed variation of $E_{1/2}$ with pH, providing similar values of E_2^f, $K_{red,1}$ and $K_{ox,2}$ for the two forms of covalently immobilized *TOP*, and somewhat higher values of the three parameters in the case of the physisorbed enzymes (see Table 1). If both A_1H and A_2H acid groups in Scheme 1 are tentatively identified as carboxylic groups, then the increase in $K_{red,1}$ and $K_{ox,2}$ would be consistent with the presence of a more polar environment around these acid groups [28], a larger exposure of the heme propionates to the solvent molecules could also explain the E_2^f positive shift of *pa-mon-TOP* according to Bortolotti et al. simulations [29].

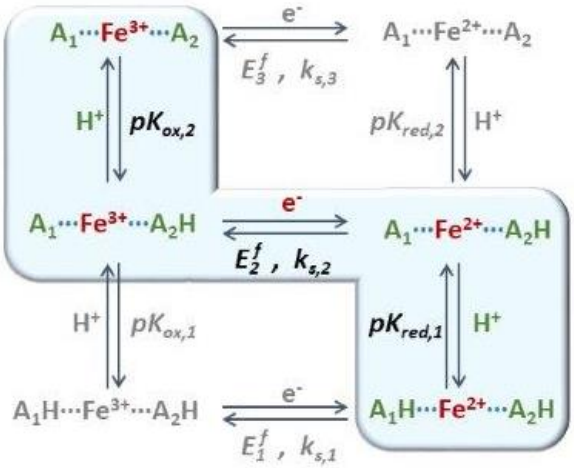

Scheme 1. Six membered ladder-scheme for a one-electron two-protons redox couple. Electrons and protons are exchanged horizontally and vertically, respectively. The shaded area highlights the reaction pathway that operates in the present working conditions.

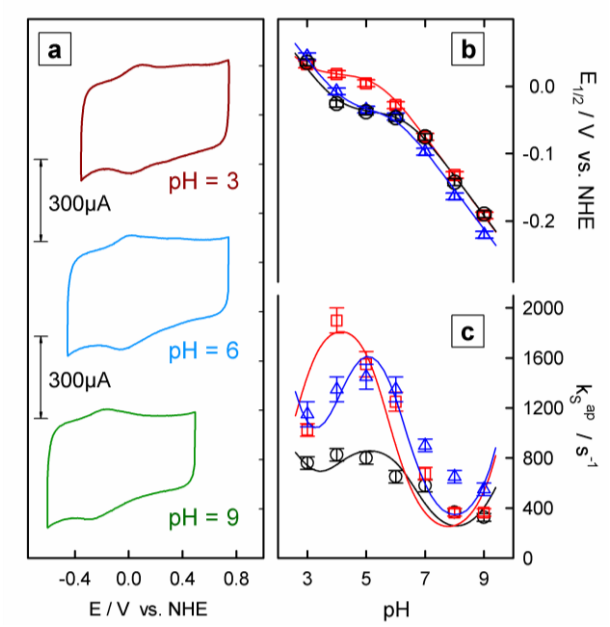

Figure 1. (a) Voltammetric response of *ci-olig-TOP* recorded at 10 V s^{-1} and the indicated pH values. (b) Variation of the midpoint potential with solution pH of *ci-olig-TOP* (black circles, ○), *ci-mon-TOP* (blue triangles, Δ) and *pa-mon-TOP* (red squares, □). (c) Variation of the apparent standard electron transfer rate constant with solution pH, symbols as in (b). Solid lines in (b) and (c) are theoretical fits to eqs. (2) and (3), respectively. Other experimental conditions: 0.02 M SPB (I = 0.12 M) and 25ºC.

Apparent standard electron transfer rate constants k_s^{ap} were derived from the variation of the voltammetric peak potential separation with the potential scan rate as described by Laviron [23], by assuming that the charge transfer coefficient equals 0.5. Figure 1c illustrates the k_s^{ap} values obtained as a function of the solution pH and the *TOP* immobilization protocol. It may be observed how the immobilization protocol affects the k_s^{ap} values mainly in acid solutions, where they reach maxima for pH values close to 5, whereas k_s^{ap} becomes nearly independent of the immobilization protocol for pH $\geq$ 7. It is interesting to note that the electrocatalytic activity of TOP [13] and HRP [30-32] has also been reported to display maxima in the vicinity of pH 5.

The pH dependence of k_s^{ap} can be expressed in terms of Scheme 1 as [26,27]:

$$k_s^{ap} = \frac{\left(Q_1\ c_{H^+}\right) + k_{s,2} + \left(Q_3 / c_{H^+}\right)}{\left(1+\left(K_{ox,2} / c_{H^+}\right)\right)^{1/2}\left(1+\left(c_{H^+} / K_{red,1}\right)\right)^{1/2}} \qquad (3)$$

where $Q_1 = k_{s,1}\left(K_{ox,1}K_{red,1}\right)^{-1/2}$, $Q_3 = k_{s,3}\left(K_{ox,2}K_{red,2}\right)^{1/2}$, and it has been assumed that $\left(c_{H^+} / K_{ox,1}\right) << 1$ and $\left(K_{red,2} / c_{H^+}\right) << 1$ as in eq. (2). The denominator of eq. (3) can be computed in a straightforward way from the $K_{ox,2}$ and $K_{red,1}$ values derived from the

$E_{1/2}$ vs. pH plots. The individual contributions of the Q_1, $k_{s,2}$ and Q_3 terms to the numerator W:

$$W = k_s^{ap}\left(1+\left(K_{ox,2}/c_{H^+}\right)\right)^{1/2}\left(1+\left(c_{H^+}/K_{red,1}\right)\right)^{1/2} = \left(Q_1\, c_{H^+}\right)+k_{s,2}+\left(Q_3/c_{H^+}\right) \quad (4)$$

vary with the solution pH, as illustrated in Figure 2. The two acidic and basic branches of the plots in Figure 2 provide estimates of Q_1 and Q_3, respectively, while the ordinate of the flat minimum located at intermediate pH values is a direct measure of $\log k_{s,2}$. The optimum Q_1, $k_{s,2}$ and Q_3 values that reproduce the observed kinetic behavior are collected in Table 1, except for the Q_1 value of physisorbed *TOP* since there is no observable acidic branch of W in this case. Though the lack of $K_{ox,1}$ and $K_{red,2}$ values prevents a more detailed analysis of Q_1 and Q_3 in terms of $k_{s,1}$ and $k_{s,3}$, the parameter values collected in Table 1 appear to support a progressive slowdown of the electron exchange between enzymes and electrode as the extent of protein crosslinking increases. To explore in more detail the consequences of the immobilization protocol, we consider in the next section the influence of temperature on the thermodynamics and kinetics of the *Fe(III)/Fe(II)* redox process.

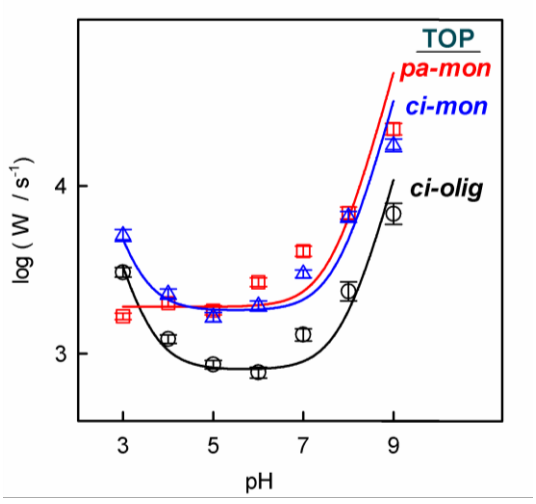

Figure 2. Logarithmic plot of the kinetic parameter *W*, defined in the text, as a function of solution pH for the three indicated immobilization protocols. Other conditions: 0.02 M SPB (I = 0.12 M) and 25ºC.

Table 1. Electron and Proton Transfer Parameters Describing the *Fe(III)/Fe(II)* Redox Conversion of Immobilized Tobacco Peroxidase at 25ºC.

	pa-mon-TOP	*ci-mon-TOP*	*ci-olig-TOP*
$pK_{Red,1}$	2.9 ± 0.2	4.3 ± 0.2	4.0 ± 0.2
$pK_{Ox,2}$	5.5 ± 0.2	6.0 ± 0.2	6.4 ± 0.2
E_2^f / mV (NHE)	18 ± 5	–36 ± 5	–38 ± 5
$k_{s,2}$ / s^{-1}	$(1.9 \pm 0.2)\cdot 10^3$	$(1.6 \pm 0.2)\cdot 10^3$	$(0.9 \pm 0.2)\cdot 10^3$
Q_1 / M^{-1} s^{-1}	-	$(3.5 \pm 0.5)\cdot 10^6$	$(2.5 \pm 0.5)\cdot 10^6$
Q_3 / M s^{-1}	$(4.5 \pm 0.5)\cdot 10^{-5}$	$(2.0 \pm 0.5)\cdot 10^{-5}$	$(1.0 \pm 0.2)\cdot 10^{-5}$

3. 2. Influence of temperature on the Fe(III) / Fe(II) redox conversion of TOP

As before, we will make use of the six membered ladder-scheme to decouple the proton and electron transfer contributions to the redox process by determining the corresponding values of $E_{1/2}$ (Figure 3) and k_s^{ap} (Figure 5) at seven equispaced temperatures in the 0-30ºC range.

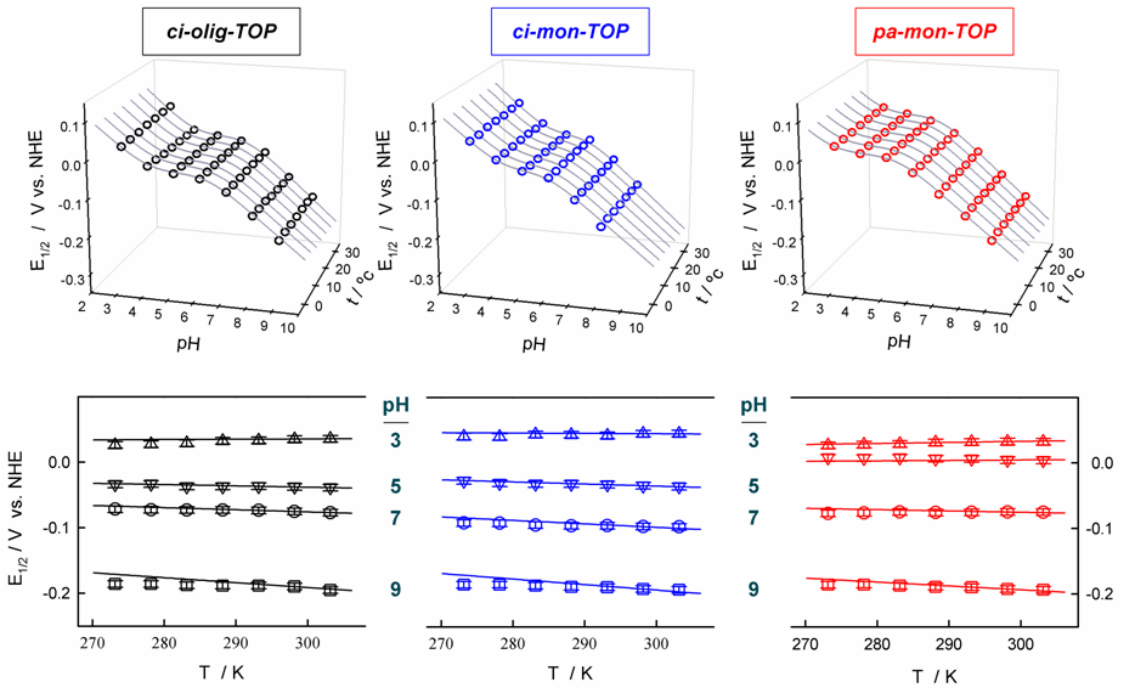

Figure 3. Midpoint potential as a function of pH and temperature for the three indicated immobilization protocols. Solid lines were computed from eq. (2), as indicated in the text. Other experimental conditions: 0.02 M SPB (I = 0.12 M).

Satisfactory fits of the $E_{1/2}$ vs pH plots in Figure 3 were derived from eq. (2) at all temperatures, by assuming that $K_{red,1}$ and $K_{ox,2}$ were independent of temperature. This assumption was further tested by inspecting the $E_{1/2}$ vs T plots at a given pH in Figure 3. It may be observed that, for any *TOP* immobilization protocol, these plots consist of a set of straight lines, whose slope becomes more negative as the solution pH increases. This behavior can be rationalized by taking derivatives in eq. (2) with respect to temperature, to obtain

$$\left(\frac{\partial E_{1/2}}{\partial T}\right)_{P,x_i} = \left(\frac{\partial E_2^f}{\partial T}\right)_{P,x_i} + \frac{R}{F}\ln\frac{\left(c_{H^+}/K_{red,1}\right)+1}{1+\left(K_{ox,2}/c_{H^+}\right)} \qquad (5)$$

where P and x_i stand for pressure and solution composition, respectively. The slope of the $E_{1/2}$ vs T plots turns out to be the sum of two contributions: the $\left(\partial E_2^f / \partial T\right)_{P,x_i}$ term, which is pH independent, and a second pH dependent term, whose value evolves from positive to negative as the solution becomes more basic, and it accounts for the change of slope observed in Figure 3.

The $\left(\partial E_2^f / \partial T\right)_{P,x_i}$ term in eq. (5) is directly related to the reduction entropy $\Delta S_{2,rc}^f$ corresponding to the electron transfer pathway 2 in Scheme 1, which can be expressed in the non-isothermal cell configuration as [33–35]:

$$\Delta S_{2,rc}^f = nF\left(\frac{\partial E_2^f}{\partial T}\right)_{P,x_i} \tag{6}$$

where n = 1 and F has its usual meaning. Analogously, the reduction enthalpy $\Delta H_{2,rc}^f$ (referred to the normal hydrogen electrode at room temperature) is given by:

$$\Delta H_{2,rc}^f = nF\left(\frac{\partial\left(E_2^f\left(\mathrm{NHE}\right)/T\right)}{\partial\left(1/T\right)}\right)_{P,x_i} \tag{7}$$

Over the limited temperature range considered here, both E_2^f vs T and E_2^f / T vs $1/T$ plots are linear (see Figures 4a and b), and the corresponding $\Delta S_{2,rc}^f$ and $\Delta H_{2,rc}^f$ values have been collected in Table 2. These values lay well within the ranges reported for peroxidases in solution at pH 7, namely, 210 J mol^{-1} K^{-1} $\leq \Delta S_{rc}^f \leq$ -120 J mol^{-1} K^{-1} and 91 kJ mol^{-1} K^{-1} $\leq \Delta H_{rc}^f \leq$ -18 kJ mol^{-1} K^{-1} [20]. It is interesting to note that the $\Delta S_{2,rc}^f$ and $\Delta H_{2,rc}^f$ values obtained for *ci-olig-TOP* and *ci-mon-TOP* are similar and negative, in stark contrast with the positive values determined for *pa-mon-TOP*. In the case of electron transfer proteins with positively charged redox centers, more positive reduction entropies are generally associated with an increase of the solvent accessibility to the

redox center [36]. Therefore, the more positive $\Delta S^{f}_{2,rc}$ value of physisorbed *TOP* enzymes suggests that they acquire a more open and solvent accessible polypeptide structure upon adsorption on graphite. On the other hand, crosslinking with the graphite surface and with other *TOP* molecules helps to preserve the native and catalytically active structure of *ci-mon-TOP* and *ci-olig-TOP*, but it also restricts the solvent access to the redox center. Extensive enthalpy-entropy compensation, as observed in Table 2 for the three immobilization protocols, points also to a substantial contribution of the solvent exchange between protein and solution to the energetics of *TOP* reduction [37].

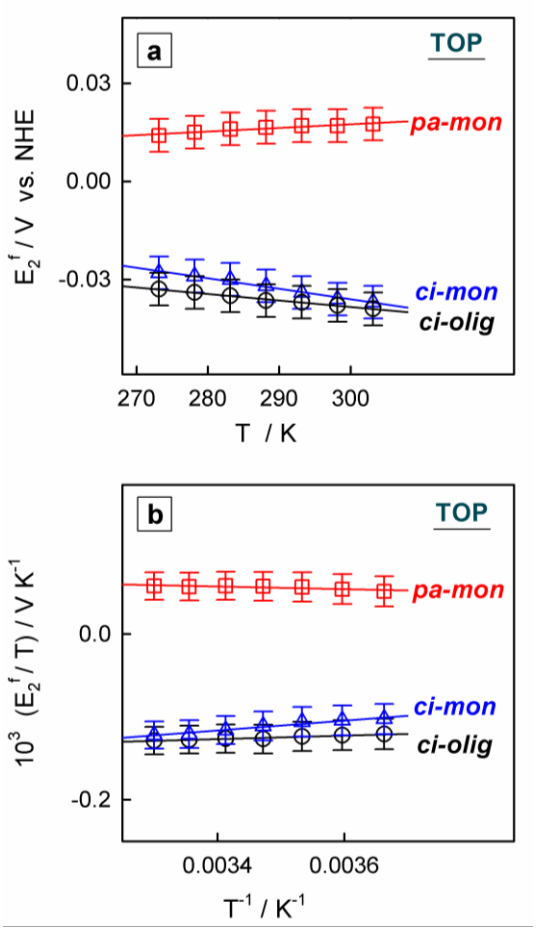

Figure 4. (a) Formal potential E_2^f vs absolute temperature T and (b) E_2^f / T vs T^{-1} plots for the three indicated immobilization protocols. Solid lines in plots (a) and (b) are linear least-squares fits. Other experimental conditions: 0.02 M SPB (I = 0.12 M).

Table 2. Thermodynamic and Kinetic Parameters Describing the Influence of Temperature on the *Fe(III) / Fe(II)* Redox Conversion of Immobilized *TOP*.

	pa-mon-TOP	*ci-mon-TOP*	*ci-olig-TOP*
$\Delta S_{2,rc}^f / J\,K^{-1}\,mol^{-1}$	13 ± 7	–37 ± 7	–24 ± 8
$\Delta H_{2,rc}^f / kJ\,mol^{-1}$	2 ± 1	–8 ± 2	–4 ± 1
$10^{-4} \cdot A_2$ / s^{-1}	23 ± 8	3.0 ± 0.9	1.7 ± 0.7
$\Delta H_2^{\neq}$ / $kJ\,mol^{-1}$	10 ± 1	5.8 ± 0.5	6.2 ± 0.5

Within the temperature range of interest, the k_s^{ap} vs pH profiles were similar to those already discussed at 25ºC (see Figure 5), and were also fitted to eq. (3) to obtain sets of optimized Q_1, $k_{s,2}$ and Q_3 values at each temperature. Both Q_1 and Q_3 displayed a stronger variation with temperature (not shown) than that of $k_{s,2}$, but we have limited our analysis to the $k_{s,2}$ values due to the impossibility of decoupling the contributions of rate and equilibrium constants to the observed variation of Q_1 and Q_3 with temperature.

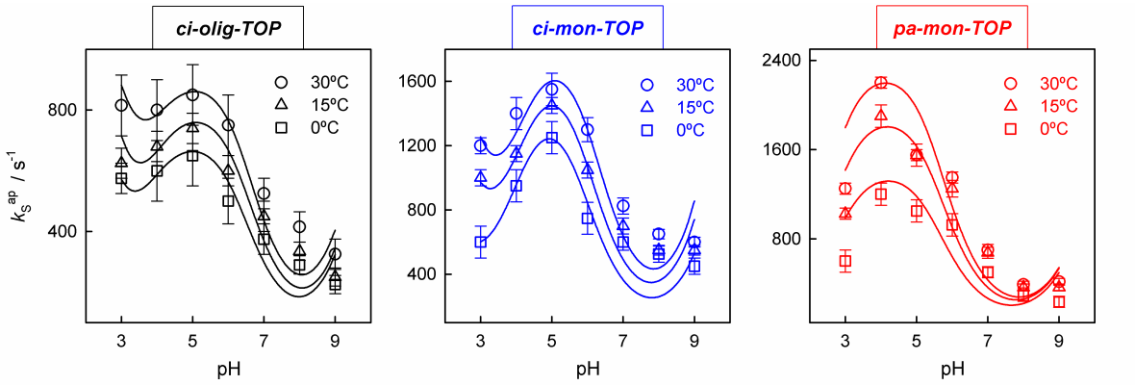

Figure 5. pH and temperature dependence of the standard electron transfer rate constant k_s^{ap} for the three indicated immobilization protocols. Solid lines are theoretical fits computed from equation (3). Other experimental conditions: 0.02 M SPB (I = 0.12 M).

The three immobilization protocols lead to linear Arrhenius plots displayed in Figure 6. The intercept and slope of these plots provide the pre-exponential factor (A_2) and activation enthalpy ($\Delta H_2^{\neq}$) for electron transfer, according to:

$$\ln k_{s,2} = \ln A_2 - \frac{\Delta H_2^{\neq}}{RT} \qquad (8)$$

A_2 and $\Delta H_2^{\neq}$ values are collected in Table 2, and both may be seen to decrease as the extent of *TOP* crosslinking increases, so that their combined values tend to mitigate the influence of the immobilization protocol on the observed rate of electron transfer. A more detailed interpretation of the A_2 and $\Delta H_2^{\neq}$ values requires the adoption of a specific electron transfer mechanism.

The rate of electron exchange between *TOP* and graphite is quite fast, in spite of the low density of electronic states of graphite (compare 0.0022 eV^{-1} for graphite [38,39] with 0.28 eV^{-1} for a typical metal like gold [40]), which reduces the probability of electron transfer between enzyme and electrode, and reinforces the possibility that this electron exchange takes place through a nonadiabatic mechanism [40]. The adequacy of

this mechanism is also supported by the observed insensitivity of the measured k_s^{ap} values to the replacement of water by a highly viscous solution as solvent (specifically, a 2.8 M glucose solution with η = 4.9 cP at 22ºC [41]). Then, within the framework of a nonadiabatic electron transfer regime [41]:

$$A_2 \propto \left|H_{AB}\right|^2 \tag{9a}$$

$$\Delta H_2^{\neq} = \frac{\lambda_2}{4} \tag{9b}$$

where H_{AB} and λ_2 are the electronic coupling and reorganization energies, respectively.

The extent of electronic coupling varies with the thickness and electronic conductivity of the intervening medium between electrode and redox center [42]. Since the immobilization protocol is not expected to induce dramatic changes in the electronic conductivity of the polypeptide matrix, the sequence of A_2 values in Table 2 is likely to reflect differences in the distance of closest approach of the heme group to the electrode, which would be then smaller for *pa-mon-TOP* than for *ci-mon-TOP* and *ci-olig-TOP*. According to this interpretation, physisorption of *TOP* enzymes would be accompanied by conformational changes that bring the heme group closer to the electrode surface. In the case of chemisorbed *TOP* enzymes, the formation of inter- and intramolecular amide bonds would help to fix the native protein structure and prevent a closer approach of the heme group to the electrode.

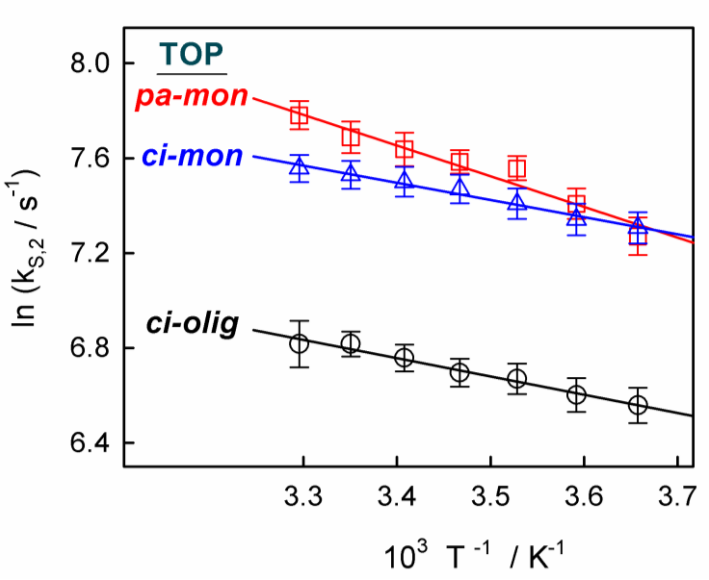

Figure 6. Arrhenius plot for the standard electron transfer rate constant $k_{s,2}$, for the three indicated immobilization protocols. Solid lines are linear least-squares fits. Other experimental conditions: 0.02 M SPB (I = 0.12 M).

The complex molecular scaffold of proteins restricts the mobility of the various dipoles (such as peptide groups or solvent molecules) that may reorient when the charge of a redox cofactor is changed in an electron transfer event, and thereby it helps to lower its reorganization energy in comparison to similar reactions involving simple reactants in solution [43]. Moreover, the immobilization of a redox protein on a surface is expected to reduce further the contribution of the surrounding medium to the reorganization energy [44,45]. Thus, the reorganization energy of cytochrome *c* has been reported to decrease from ~0.6 eV in solution down to ~0.3 eV in the adsorbed state [46]. This last value is close to the reorganization energies derived from the $\Delta H_2^{\neq}$ values collected in Table 2, i. e.: 0.23 eV for *ci-mon-TOP*, 0.25 eV for *ci-olig-TOP* and 0.41 eV for physisorbed *TOP*. The higher value obtained for physisorbed *TOP* is again consistent with an easier access of the solvent to the redox center and its involvement in

the activation process [47,48], whereas the lower values determined for covalently immobilized proteins can be considered as a direct consequence of the more rigid and tight molecular envelope that crosslinking generates around the redox center [43].

3. Conclusions

In this work we have shown how the *Fe(III)/Fe(II)* redox couple of tobacco peroxidase can be used to probe the energetics and electronic connectivity of the heme pocket. Analysis of the combined effects of pH and temperature on the voltammetric response leads to a detailed interpretation of the influence of the enzyme immobilization protocol on its electrochemical behavior. As compared with covalently immobilized *TOP*, physisorbed enzymes are characterized by a more positive reduction entropy and a higher reorganization energy, which are indicative of a more extensive solvent involvement in the electron transfer process. These observations, together with a larger electronic coupling between heme and electrode point to a partial denaturation of the physorbed *TOP* enzymes as the origin of their low electrocatalytic activity. Thermodynamic parameter values are similar for covalently immobilized monomers and oligomers, while a larger electronic coupling is responsible for the somewhat higher electron transfer rate constants determined for the monomers. However, intermolecular crosslinking results in a higher population of electroactive oligomers and, overall, in a more active electrocatalytic film.

Acknowledgements

J. L. O., J. J. C. and R. A. acknowledge financial support from the Spanish Ministry of Economy and Competitiveness and the European Union FEDER (grants CTQ2014-

52641-P and CTQ2015-71955-REDT (ELECTROBIONET)) and L. G. from the Swedish Research Council (grant 2014-5908).

References

[1] H. B. Dunford, *Heme Peroxidases*, John Wiley, Chichester, 1999.

[2] I. G Gazaryan, L. M. Lagrimini, Purification and Unusual Kinetic Properties of a Tobacco Anionic Peroxidase, Phytochem. 41 (1996) 1029-1034.

[3] I. G. Gazaryan, L. Gorton, T. Ruzgas, E. Csöregi, W. Schuhmann, L. M Lagrimini, D. M. Khushpulian, V. I. Tishkov, Tobacco Peroxidase as a New Reagent for Amperometric Biosensors, J. Anal. Chem. 60 (2005) 558–566.

[4] C. Léger, P. Bertrand, Direct Electrochemistry of Redox Enzymes as a Tool for Mechanistic Studies, Chem. Rev. 108 (2008) 2379-2438.

[5] U. Wollenberger, Third generation biosensors – integrating recognition and transduction in electrochemical sensors. In *Biosensors and Modern Biospecific Analytical Techniques*, L. Gorton Ed.; Elsevier: Amsterdam, 2005; pp 65-130.

[6] L. Betancor, H. R. Luckarift, Enzyme Immobilization for Biological Fuel Cell Applications. In *Enzymatic Fuel Cells: from Fundamentals to Applications*, H. R. Luckarift, P. Atanassov and G. R. Johnson Eds.; Wiley: Hoboken, 2014; pp. 208-224.

[7] F. D. Munteanu, A. Lindgren, J. Emnéus, L. Gorton, T. Ruzgas, E. Csöregi, A. Ciucu, R. B. Van Huystee, I. G. Gazaryan, L. M. Lagrimini, Bioelectrochemical Monitoring of Phenols and Aromatic Amines in Flow Injection Using Novel Plant Peroxidases, Anal. Chem. 70 (1998) 2596-2600.

[8] F. D. Munteanu, L. Gorton, A. Lindgren, T. Ruzgas, J. Emnéus, E. Csöregi, I. G. Gazaryan, I. V. Ouporov, E. A. Mareeva, L. M. Lagrimini, Direct and Mediated Electron Transfer Catalyzed by Anionic Tobacco Peroxidase, Appl. Biochem. Biotechnol. 88 (2000) 321-333.

[9] A. Lindgren, T. Ruzgas, L. Gorton, E. Csöregi, G. B. Ardila, I. Y. Sakharov, I. G. Gazaryan, Biosensors Based on Novel Peroxidases with Improved Properties in Direct and Mediated Electron Transfer, Biosens. Bioelectron. 15 (2000) 491–497.

[10] S. Gaspar, I. C. Popescu, I. G. Gazaryan, A. G. Bautista, I. Y. Sakharov, B. Mattiasson, E. Csöregi, Biosensors Based on Novel Plant Peroxidases: a Comparative Study, Electrochim. Acta 46 (2000) 255–264.

[11] S. Gaspar, H. Zimmermann, I. G. Gazaryan, E. Csöregi, W. Schuhmann, Hydrogen Peroxide Biosensors Based on Direct Electron Transfer from Plant Peroxidases Immobilized on Self-Assembled Thiol-Monolayer Modified Gold Electrodes, Electroanalysis 13 (2001) 284-288.

[12] E. E. Ferapontova, J. Castillo, D. M. Hushpulian, V. I. Tishkov, T. Chubar, I. G. Gazaryan, L. Gorton, Direct Electrochemistry of Recombinant Tobacco Peroxidase on Gold, Electrochem. Commun. 7 (2005) 1291–1297.

[13] J. Castillo, E. E. Ferapontova, D. M. Hushpulian, F. Tasca, V. Tishkov, T. Chubar, I. G. Gazaryan, L. Gorton, Direct Electrochemistry and Bioelectrocatalysis of H_2O_2 Reduction of Recombinant Tobacco Peroxidase on Graphite. Effect of Peroxidase Single-point Mutation on Ca^{2+}-modulated Catalytic Activity, J. Electroanal. Chem. 588 (2006) 112–121.

[14] J. L Olloqui-Sariego, G. S. Zakharova, A. A. Poloznikov, J. J. Calvente, D. M. Hushpulian, L. Gorton, R. Andreu, Interprotein Coupling Enhances the Electrocatalytic Efficiency of Tobacco Peroxidase Immobilized at a Graphite Electrode, Anal. Chem. 87 (2015) 10807-10814.

[15] J. L Olloqui-Sariego, G. S. Zakharova, A. A. Poloznikov, J. J. Calvente, D. M. Hushpulian, L. Gorton, R. Andreu, Fenton-like Inactivation of Tobacco Peroxidase Electrocatalysis at Negative Potentials, ACS Catal. 6 (2016) 7452-7457.

[16] P. Bollella, L. Medici, M. Tessema, A. A. Poloznikov, D. Hushpulian, V. I. Tishkov, R. Andreu, D. Leech, N. Megersa, M. Marcaccio, L. Gorton, R. Antiochia, Highly Sensitive, Stable and Selective Hydrogen Peroxide Amperometric Biosensors Based on Peroxidases from Different Sources Wired by Os-polymer: A Comparative Study. Solid State Ionics 314 (2018) 178-186.

[17] F. A. Armstrong, Recent Developments in Dynamic Electrochemical Studies of Adsorbed Enzymes and their Active Sites, Curr. Opin. Chem. Biol. 9 (2005) 110–117.

[18] M. S. Mondal, H. A. Fuller, F. A. Armstrong, Direct Measurement of the Reduction Potential of Catalytically Active Cytochrome *c* Peroxidase Compound I: Voltammetric Detection of a Reversible, Cooperative Two-Electron Transfer Reaction, J. Am. Chem. Soc. 118 (1996) 263–264.

[19] G. P. Stevenson, C.-Y. Lee, G. F. Kennedy, A. Parkin, R. E. Baker, K. Gillow, F. A. Armstrong, D. J. Gavaghan, A. M. Bond, Theoretical Analysis of the Two-Electron Transfer Reaction ans Experimental Studies with Surface-Confined Cytochrome c Peroxidase Using Large-Amplitude Fourier Transformed AC Voltammetry, Langmuir 28 (2012) 9864–9877.

[20] G. Battistuzzi, M. Bellei, C. A. Bortolotti, M. Sola, Redox Properties of Heme Peroxidases, Arch. Biochem. Biophys. 500 (2010) 21–36.

[21] D. M. Hushpulian, P. A. Savitski, A. M. Rojkova, T. A. Chubar, V. A. Fechina, I. Y. Sakharov, L. M. Lagrimini, V. I. Tishkov, I. G. Gazaryan, Expression and Refolding of Tobacco Anionic Peroxidase from *E. coli* Inclusion Bodies, Biochem.(Moscow) 68 (2003) 1189–1194.

[22] I. G. Gazaryan, L. M. Lagrimini, S. J. George, R. N. Thorneley, Anionic Tobacco Peroxidase is Active at Extremely Low pH: Veratryl Alcohol Oxidation with a pH Optimum of 1.8, Biochem. J. 320 (1996) 369–372.

[23] E. Laviron, General Expression of the Linear Potential Sweep Voltammogram in the Case of Diffusionless Electrochemical Systems, J. Electroanal. Chem. 101 (1979) 19–28.

[24] H. H. Harbury, Oxidation-Reduction Potentials of Horseradish Peroxidase, J. Biol. Chem. 225 (1957) 1009–1024.

[25] H. Yamada, R. Makino, I. Yamazaki, Effects of 2,4-Substituents of Deuteroheme upon Redox Potentials of Horseradish Peroxidases, Arch. Biochem. Biophys. 169 (1975) 344–353.

[26] E. Laviron, Electrochemical Reactions with Protonations at Equilibrium. Part III. The 1e, 2 H^+ Reaction (Six-Member Ladder Scheme) for a Surface or for a Heterogeneous Reaction, J. Electroanal. Chem. 124 (1981) 9-17.

[27] H. O. Finklea, Theory of Coupled Electron-Proton Transfer with Potential-Dependent Transfer Coefficients for Redox Couples Attached to Electrodes, J. Phys. Chem. B, 105 (2001) 8685-8693.

[28] C. N. Pace, G. R. Grimsley,J. M. Scholtz, Protein Ionizable Groups: p*K* Values and Their Contribution to Protein Stability, J. Biol. Chem. 284 (2009) 13285-13289.

[29] C. A. Bortolotti, A. Amadei, M. Aschi, M. Borsari, S. Corni, M. Sola, I. Daidone The Reversible Opening of Water Channels in Cytochrome c Modulates the Heme Iron Reduction Potential, J. Am. Chem. Soc. 134 (2012) 13670-13678.

[30] E. E. Ferapontova, L. Gorton, Effect of Proton Donors on Direct Electron Transfer in the System Gold Electrode-Horseradish Peroxidase, Electrochem. Commun. 3 (2001) 767–774.

[31] E. E. Ferapontova, L. Gorton, Effect pf pH on Direct Electron Transfer in the System Gold Electrode-Recombinant Horseradish Peroxidase, Bioelectrochem. 55 (2002) 83–87.

[32] R. Andreu, E. E. Ferapontova, L. Gorton, J. J. Calvente, Direct Electron Transfer Kinetics in Horseradish Peroxidase Electrocatalysis, J. Phys. Chem. B 111 (2007) 469-477.

[33] E. L. Yee, R. J. Cave, K. L. Guyer, P. D. Tyma, M. J. Weaver, A Survey of Ligand Effects upon the Reaction Entropies of Some Transition Metal Redox Couples, J. Am. Chem. Soc. 101 (1979) 1131-1137.

[34] V. T. Taniguchi, N. Sailasuta-Scott, F. C. Anson, H. B. Gray, Thermodynamics of Metalloprotein Electron Transfer Reactions, Pure & Appl. Chem. 52 (1980) 2275-2281.

[35] G. Battistuzzi, M. Borsari, M. Sola, Medium and Temperature Effects on the Redox Chemistry of Cytochrome *c*, Eur. J. Inorg. Chem. (2001) 2989-3004.

[36] G. Battistuzzi, M. Bellei, M. Borsari, G. W. Canters, E. de Waal, L. J. C. Jeuken, A. Ranieri, M. Sola, Control of Metalloprotein Reduction Potential: Compensation Phenomena in the Reduction Thermodynamics of Blue Copper Proteins, Biochemistry 42 (2003) 9214-9220.

[37] E. Grunwald, C. Steel, Solvent Reorganization and Enthalpy-Entropy Compensation, J. Am. Chem. Soc. 117 (1995) 5687-5692.

[38] H. Gerischer, R. McIntyre, D. Scherson, W. Storck, Density of the Electronic States of Graphite: Derivation from Differential Capacitance Measurements, J. Phys. Chem. 91 (1987) 1930–1935.

[39] R. L. McCreery, Advanced Carbon Electrode Materials for Molecular Electrochemistry, Chem. Rev. 108 (2008) 2646–2687.

[40] W. Schmickler, J. Mohr, The Rate of Electrochemical Electron-Transfer Reactions, J. Chem. Phys. 117 (2002) 2867–2872.

[41] J. L. Olloqui-Sariego, B. Moreno-Beltrán, A. Díaz-Quintana, M. A. De la Rosa, J.J. Calvente, R. Andreu, Temperature-Driven Changeover in the Electron-Transfer Mechanism of a Thermophilic Plastocyanin, J. Phys. Chem. Lett. 5 (2014) 910–914.

[42] J. R. Winkler, H. B. Gray, Electron Flow through Metalloproteins, Chem. Rev. 114 (2014) 3369–3380.

[43] L. I. Krishtalik, The Medium Reorganization Energy for the Charge Transfer Reactions in Proteins, Biochim. Biophys. Acta 1807 (2011) 1444–1456.

[44] Y. –P. Liu, M. D. Newton, Reorganization Energy for Electron Transfer at Film-modified Electrode Surfaces: a Dielectric Continuum Model, J. Phys. Chem. 98 (1994) 7162–7169.

[45] S. Terrettaz, J. Chung, C. J. Miller, Kinetic Parameters for Cytochrome *c* via Insulated Electrode Voltammetry, J. Am. Chem. Soc. 118 (1996) 7857–7858.

[46] D. Alvarez-Paggi, L. Hannibal, M. A. Castro, S. Oviedo-Rouco, V. Demicheli, V. Tórtora, F. Tomasina, R. Radi, D. H. Murgida, Multifunctional Cytochrome *c*: Learning New Tricks from an Old Dog, Chem. Rev. 117 (2017) 13382–13460.

[47] H. Shafiey, H. Ghourchian, N. Mogharrab, How Does Reorganization Energy Change upon Protein Unfolding? Monitoring the Structural Perturbations in the Heme Cavity of Cytochrome *c*, Biophys. Chem. 134 (2008) 225–231.

[48] C. A. Bortolotti, M. E. Siwko, E. Castellini, A. Ranieri, M. Sola, S. Conti, The Reorganization Energy in Cytochrome *c* is Controlled by the Accesibility of the Heme to the Solvent, J. Phys. Chem. Lett. 2 (2011) 1761–1765.

Highlights

- The *Fe(III)/Fe(II)* redox couple of tobacco peroxidase is used to probe the energetics and electronic connectivity of the electrocatalytic heme pocket.
- The proposed probe is used to dissect the influence of the enzyme immobilization protocol on the electrocatalytic activity.
- Charge transfer thermodynamic and kinetic parameters are obtained as a function of temperature and pH.
- Reduction entropies and reorganization energies are markedly different for physisorbed and covalently immobilized enzymes.
- The electronic coupling between heme and electrode decreases as the extent of enzyme crosslinking increases.

Graphical Abstract